# Pore Formation in Poly(divinylbenzene) Networks Derived from Organotellurium-Mediated Living Radical Polymerization

**Joji Hasegawa,[†] Kazuyoshi Kanamori,*[,†] Kazuki Nakanishi,[†] Teiichi Hanada,[†] and Shigeru Yamago[‡]**

*Department of Chemistry, Graduate School of Science, Kyoto University, Kitashirakawa, Sakyo-ku, Kyoto 606-8502, Japan, and Institute for Chemical Research, Kyoto University, Uji, 611-0011, Japan*

*Received October 17, 2008; Revised Manuscript Received December 17, 2008*

ABSTRACT: Macroporous cross-linked polymeric dried gels have been obtained by inducing phase separation in a homogeneous poly(divinylbenzene) (PDVB) network formed by organotellurium-mediated living radical polymerization (TERP). The living polymerization reaction of DVB with the coexistence of a nonreactive polymeric agent, poly(dimethylsiloxane) (PDMS), in solvent 1,3,5-trimethylbenzene (TMB) resulted in polymerization-induced phase separation (spinodal decomposition), and the transient structure of spinodal decomposition has been frozen by gelation. Well-defined macroporous monolithic dried gels with bicontinuous structure in the micrometer scale are obtained after removing PDMS and TMB by simple washing and drying. Inside the skeletons that comprise the macroporous structure, "skeletal pores" with various sizes in nanometer scale have also been found by gas sorption measurements. The skeletal pores are deduced to be formed by secondary phase separation in the skeletons due to the thermodynamic instability that arises in the separated phases during the polymerization. The properties of the macropores and the skeletal pores have been controlled by changing starting composition, molecular weight of PDMS, and reaction temperature.

## 1. Introduction

In order to realize a better control of the structural and morphological nature of polymers, controlled living radical polymerization techniques have been intensively studied. Since the ideal living polymerization does not allow termination and chain transfer reactions but only allow initiation and propagation reactions, propagating ends are still reactive, or "living", even after all of the monomers are consumed. The following unique features are observed as a result of living polymerization.[1] (1) The number average molecular weight $M_n$ proportionally increases with the progress of the monomer conversion, and $M_n$ is also proportional to the initial monomer/initiator ratio. This allows the fine control of molecular weight by adequately changing the monomer/initiator ratio. (2) Due to the livingness of the system, additional supply of monomers to the system in which all monomers have been completely consumed evokes further polymerization. Polymers with defined structure such as block polymers, grafted polymers and star polymers etc. can be precisely synthesized by utilizing the livingness. (3) The $M_w/M_n$ ratio, or the polydispersity index (PDI), can be close to unity. From these three features, it has become possible to universally control the dispersity and structures of polymers in various sizes such as molecular and meso- or macroscopic levels.

In addition to the linear polymers, the nature of cross-linked polymer gels prepared by living polymerization techniques is also studied.[2−9] It is well-known that the conventional free radical polymerization leads to heterogeneous networks due to the abrupt increase of degree of polymerization (DP) resulted from slow initiation and fast chain propagation/termination reactions, which consequentially leads to a relatively broad distribution of DP. Frequent intermolecular and intramolecular cyclization reactions are also responsible for the heterogeneous networks. Such reaction characteristics generate regions with significantly higher cross-linking density compared to other regions in the network which eventually results in microgel formation.[10−14] In some cases of solution polymerization using a cross-linker, such highly cross-linked regions, or microgels, will segregate from the solution to form particle-aggregated morphology in the micrometer scale even in good solvent. Monolithic porous gels are obtained after drying as a result of microgel segregation.[15] On the contrary, living polymerization is found to give more homogeneous cross-linked structures in a gel network. Ide et al. demonstrated that the nitroxide-mediated living radical polymerization of the mixture of monovinyl and divinyl compounds leads to the formation of a highly homogeneous cross-linking and the number of cross-links at the gel point was enough close to what is predicted by the Flory-Stockmayer (FS) theory.[2,3] Contrarily, number of cross-links of the conventional free radical system is much larger due to the formation of substantial dead polymers and closed rings that do not participate in the network. Jiang et al. also confirmed the similar gelation behavior using cross-linking methacrylates by atom transfer radical polymerization (ATRP).[4,6,9]

The heterogeneous networks formation by the conventional free radical polymerization is widely applied to prepare porous polymeric materials (polymer monoliths).[16−18] Using "porogen", which is usually poor solvent for the network-forming components, results in the substantial heterogeneity in the network, and thus phase separation of microgels in the porogen is induced. The resultant morphology is composed of aggregated-microgels (particles) and the solvent (porogen). In this way the porous structure can be obtained after removal of the solvent. Polymer monoliths thus prepared are applied especially to liquid-phase separation or reaction media.[19,20] However, a fine-tuning of pore properties such as pore size, pore volume and morphology is relatively difficult because the pores are formed in-between segregated microgel particles that aggregate at random. For the purpose of improved efficiency in such applications, the pore properties should be adequately controlled.

Recently we reported the fine control of pore properties of polymer monoliths by nitroxide-mediated living radical polymerization (NMP) of divinylbenzene (DVB)[21] and by ATRP of 1,3-glycerol dimethacrylate (GDMA).[22] Both techniques are

* Corresponding author. Telephone/Fax: +81-75-753-7673. E-mail: kanamori@kuchem.kyoto-u.ac.jp.
[†] Department of Chemistry, Graduate School of Science, Kyoto University.
[‡] Institute for Chemical Research, Kyoto University.

10.1021/ma802343a CCC: $40.75 
Published on Web 01/23/2009

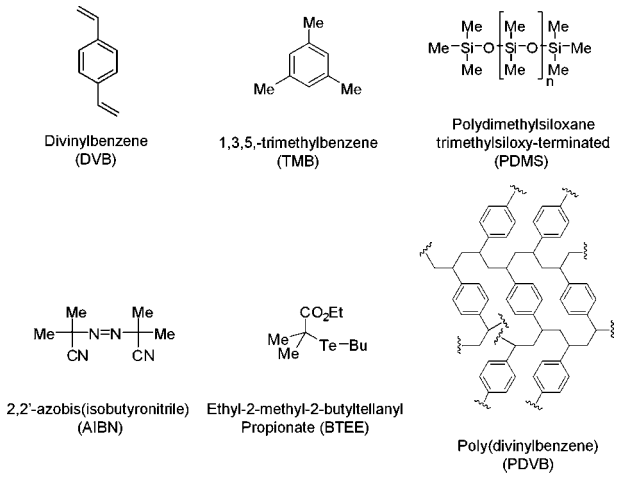


**Figure 1.** Chemical structures of the reagents and the resulting polymer.

based on polymerization-induced phase separation by spinodal decomposition in the course of the homogeneous network formation by living polymerization. Copresence of an unreactive polymeric agent in the polymerization solution induces spinodal decomposition in the course of gelation to give a well-defined bicontinuous porous structure. Pore size and pore volume are found to be independently controlled by changing the starting composition.[21] Since the more homogeneous macroporous morphology with bicontinuous structure obtained from spinodal decomposition will improve the liquid transport throughout the media, liquid-phase applications such as chromatography and catalyst supports are expected. Spinodal decomposition can be induced only in the homogeneous network otherwise the heterogeneity hinders the occurrence and development of the isotropic compositional fluctuation.[22]

In this study, organotellurium-mediated radical polymerization (TERP)[23−26] is for the first time applied to prepare polymer monoliths based on spinodal decomposition. The TERP technique, as well as ATRP and reversible addition-fragmentation chain transfer (RAFT) etc., is known as one of the versatile living radical polymerization techniques which affords well-defined linear polymers.[27] Using DVB as a monomer, poly(dimethylsiloxane) (PDMS) as a polymeric agent, and 1,3,5-trimethylbenzene (TMB) as solvent, phase separation behavior is investigated especially when changing the various parameters in the starting composition such as molecular weight of PDMS and organotellurium promoter/initiator ratio etc. The formation mechanism of mesopores inside phase-separated DVB-rich gelling phase is also discussed from physicochemical point of view.

## 2. Experimental Section

Divinylbenzene (DVB) (80% mixture of isomers) was purchased from Sigma-Aldrich Co. (USA). The solvent 1,3,5-trimethylbenzene (TMB) was purchased from Kishida Chemical Co., Ltd. (Japan). Polydimethylsiloxane (PDMS) (trimethylsiloxy-terminated, molecular weight $M_w$ = 9000−10 000 (DMS-T22, denoted as PDMS-10k), $M_w$ = 60 000−65 000 (DMS-T41, denoted as PDMS-65k)) and 2,2′-azobis(isobutyronitrile) (AIBN) were purchased from Gelest, Inc. (USA) and Tokyo Chemical Industry Co., Ltd. (Japan), respectively. Ethyl-2-methyl-2-butyltellanyl propionate (BTEE) was kindly supplied from Otsuka Chemical Co., Ltd. (Japan). All chemicals were used as received.

The chemical structure of the reagents and the resultant schematic polymer network are shown in Figure 1 and sample gels were prepared with the starting compositions listed in Table 1 as follows. Given amounts of PDMS, TMB, and DVB were mixed in a glass tube in the listed order. After stirring for ca. 3 min, the resultant homogeneous solution was degassed by ultrasonication for 3 min, and then AIBN was dissolved followed by purging with nitrogen supplied using a stainless-steel needle through a silicone resin septum for 10 min. After BTEE was added through another needle, the starting solution was transferred to an ampule and kept at 80 or 120 °C to allow the decomposition of AIBN into free radicals. Simultaneously, the living radical polymerization was allowed to proceed at the same temperature. TERP relies on the reversible generation of active carbon-centered radical species (P•) from the dormant species (P-TeBu) as in Scheme 1. After reacted for 24 h, the resultant wet gels were washed with tetrahydrofuran (THF) to remove the solvent, phase separator, and unreacted monomers, followed by evaporative drying at 60 °C for 24 h. We confirmed by elemental analysis of the dried samples that all of the included PDMS was effectively removed by the washing with THF. For the mercury porosimetry, and nitrogen sorption measurements described below, the gels were heat-treated by raising the temperature from room temperature to 150 °C in 2 h and kept for 6 h in air.

**Table 1. Starting Compositions Investigated in This Study**[a]

| code | DVB/mL | TMB/mL | PDMS-10k/g | PDMS-65k/g |
|---|---|---|---|---|
| L600-6[b] | 5 | 6 | 0.600 | |
| L600-8 | 5 | 8 | 0.600 | |
| L700-8 | 5 | 8 | 0.700 | |
| L750-8 | 5 | 8 | 0.750 | |
| L800-8 | 5 | 8 | 0.800 | |
| L825-8 | 5 | 8 | 0.825 | |
| L800-9 | 5 | 9 | 0.800 | |
| L700-10[c] | 5 | 10 | 0.700 | |
| L750-10 | 5 | 10 | 0.750 | |
| L800-10 | 5 | 10 | 0.800 | |
| L850-10 | 5 | 10 | 0.850 | |
| L900-10 | 5 | 10 | 0.900 | |
| L925-10 | 5 | 10 | 0.925 | |
| H350-16 | 5 | 16 | | 0.350 |
| H400-16[d] | 5 | 16 | | 0.400 |
| H450-16 | 5 | 16 | | 0.450 |
| H500-16 | 5 | 16 | | 0.500 |
| H525-16 | 5 | 16 | | 0.525 |
| H600-16 | 5 | 16 | | 0.600 |

[a] Each polymerization was carried out with 1 mol % BTEE and 0.5 mol % AIBN with respect to DVB otherwise noted. Reaction temperatures were, respectively, 80 and 120 °C for "L" and "H" series, unless otherwise noted. [b] 0.5 mol % BTEE was used. [c] 2 mol % BTEE was used. [d] The reaction temperature was 80 °C.

**Scheme 1. TERP, Which Relies on the Reversible Generation of Active Carbon-Centered Radical Species (P•) from the Dormant Species (P-TeBu)**

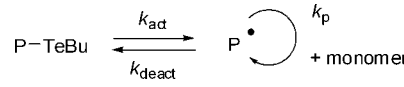


The microstructures of the fractured surfaces of the dried gels were observed by SEM (JSM-6060S, JEOL, Japan) and FE-SEM (JSM-6700F, JEOL, Japan). A mercury porosimeter (Pore Master 60-GT, Quantachrome Instruments, USA) was used to characterize the macropores of the heat-treated gels, while nitrogen adsorption−desorption (Belsorp mini II, Bel Japan, Inc., Japan) was employed to characterize the meso- and micropores of the gels. For mercury porosimetry, the pore size was characterized using the Washburn equation assuming a cylindrical shape for the pores. For nitrogen adsorption−desorption, the pore size distribution and surface area were respectively calculated by the BJH method using the adsorption branch of each isotherm and the BET method. The heat-treated samples were degassed at 110 °C under vacuum for at least 1 h prior to each measurement.

## 3. Results and Discussion

**3.1. Macropore Formation by Polymerization-Induced Phase Separation.** By TERP, we obtained transparent or translucent PDVB wet gels without adding PDMS. The trans-

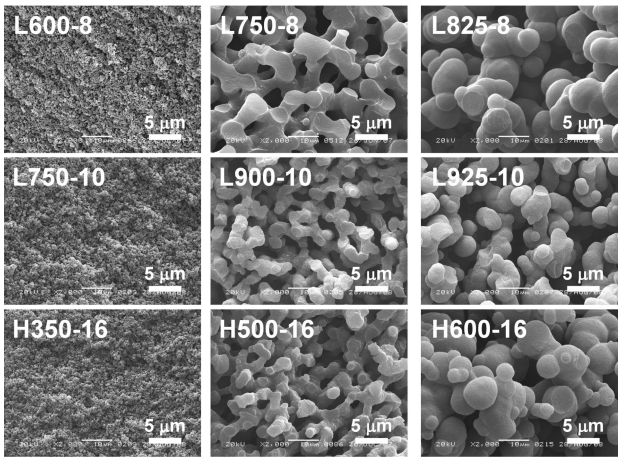


**Figure 2.** SEM images of the samples. The pore structure becomes coarser with increasing amount of PDMS (from left to right in each row). Increasing amount of TMB requires the larger [PDMS]/[DVB] ratio to obtain the comparable morphology. Conversely, the [PDMS]/[DVB] ratio is smaller in the case of the system containing PDMS with higher molecular weight.

parent or translucent PDVB wet gels turned into nonporous PDVB dried gels after evaporative drying. This implies a narrow distribution of molecular weight just before the gelation, and therefore the resultant PDVB networks are highly homogeneous in terms of the distribution of cross-linking points.[2,3,5] As has been discussed by many researchers, the abrupt reaction nature of conventional free radical polymerizations leads to heterogeneous networks containing a heterogeneous distribution of cross-linking points, which may lead to the microgel formation. This phenomenon has been widely used for conventionally tailoring porous polymer monoliths because pores are spontaneously formed in-between particles of segregated microgels even without a phase-separator[15] as described in the introductory section. On the other hand, the networks derived from living polymerizations are generally highly homogeneous.[2−9] The nonporous nature means no trace of phase separation in the course of polymerization of DVB without PDMS in the present case. With incorporating PDMS in the starting solution, porous PDVB gels with various morphologies of porous microstructure attributed to spinodal-type phase separation are obtained as reported previously.[21,22]

Figure 2 shows the SEM images of representative PDVB gels prepared from various starting compositions as listed in Table 1. Here we define sample notations as L*x*-*y* or H*x*-*y*, where "L" and "H" stand for PDMS with different molecular weights, i.e., DMS-T22 (PDMS-10k) and -T41 (PDMS-65k), respectively. The numbers *x* and *y* are the mass of PDMS in mg and volume of TMB in mL in the starting solution, respectively. The amounts of BTEE and AIBN are fixed as 0.080 mL (1 mol % of DVB) and 0.029 g (0.5 mol % of DVB) otherwise noted. Also, the reaction temperature is 80 °C for PDMS-10k system and is 120 °C for PDMS-65k system otherwise noted. The reason why we employed the higher temperature for PDMS-65k system is that the compositional area with bicontinuous structure of the gels reacted at 80 °C was considerably smaller than that of the gels reacted at 120 °C because of the larger phase separation tendency. The difference between two reaction temperatures in PDMS-65k system will be discussed in section 3.2. In the top row of Figure 2, it is presented that the well-defined bicontinuous structure develops with increasing amounts of PDMS (PDMS-10k) in the same way as previously reported in NMP and ATRP systems.[21,22] With further increasing PDMS, the bicontinuous morphology transforms into that with aggregation of particles. This obviously is resulted from the breakage of continuous gelling skeletons driven by the interfacial energy.[28,29] With increasing TMB while fixing PDMS, the macroporous morphology becomes finer, suggesting TMB is good solvent that enhances mutual compatibility of PDVB and PDMS. As shown in the middle row in Figure 2, the higher [PDMS]/[DVB] ratio in the starting solution is required to obtain the comparable morphology. When PDMS with larger molecular weight (PDMS-65k) is employed, the compositional area where PDVB gels with bicontinuous structure can be obtained shifts toward the higher concentration of TMB as shown in the bottom row of Figure 2 and Figure 3 (note that the compositional areas shown in parts a (for PDMS-10k) and b (for PDMS-65k) are different). Besides, the [PDMS]/[DVB] ratio that is required to obtain the similar structure is smaller as discussed later. With the larger molecular weight of PDMS, the demixing tendency of PDVB and PDMS becomes stronger due to the loss of entropy of mixing. Phase separation tendency of the system therefore becomes higher with increasing molecular weight of PDMS. In order to adequately control pore morphology induced by phase separation, more TMB is required to suppress the phase separation tendency.

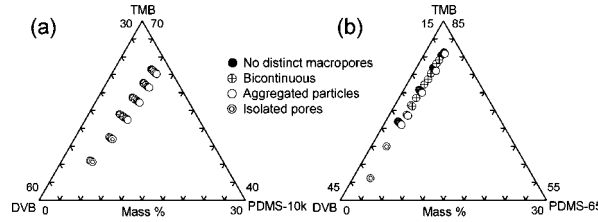


**Figure 3.** Triangular plots showing composition-morphology relationships with varying molecular weight of PDMS: (a) PDMS-10k and (b) PDMS-65k. The reaction temperatures are (a) 80 °C and (b) 120 °C.

The PDVB polymers become less soluble, i.e., a system becomes thermodynamically unstable, upon polymerization of DVB, and the originally single phase solution separates into PDVB-rich and PDMS-rich phases. This situation can be explained by the mean field theory,[30] where the change in the free energy of mixing, $\Delta G$ becomes

$$\Delta G \propto RT\left(\frac{\phi_1}{P_1}\ln\phi_1+\frac{\phi_2}{P_2}\ln\phi_2+\chi_{12}\phi_1\phi_2\right) \quad (1)$$

Here, $\phi_i$ and $P_i$ ($i = 1,2$) denote the volume fraction and degree of polymerization of component $i$, $\chi_{12}$ shows the interaction parameter, and $R$ and $T$ are the gas constant and temperature, respectively. We neglect TMB here because it only acts as a diluting agent to reduce repulsive interaction between PDVB and PDMS. So we assume the components 1 and 2 as PDVB and PDMS, respectively, in a quasibinary system. With the progress of polymerization of DVB, i.e., when $P_1$ increases, the free energy of mixing $\Delta G$ also increases (note that $\ln \phi_i$ is always negative). Phase separation takes place when $\Delta G$ becomes positive (polymerization-induced phase separation). It should be noted that, due to the large difference in solubility parameters ($\sim$9.1 cal$^{1/2}\cdot$cm$^{-3/2}$ for polystyrene-*co*-divinylbenzene and $\sim$7.3 cal$^{1/2}\cdot$cm$^{-3/2}$ for PDMS),[31,32] there is almost no miscible compositional region in PS/PDMS blends except for oligomer−oligomer blends.[33] In other words, PDVB and PDMS are extremely immiscible due to the significant enthalpic disadvantage upon mixing; the contribution from the loss of the mixing entropy is rather small. According to de Gennes,[34] in the course of polymerization, the correlation in between DVB-derived species become stronger, which is equivalent to the increase of correlation in the course of physical cooling, i.e. decreasing the temperature. Thus, increasing chemical bonds in an isothermal condition can be equivalently treated as the physical cooling and are termed as the "chemical cooling".

Now let us consider the thermodynamic instability induced by polymerization using schematic phase diagram depicted in

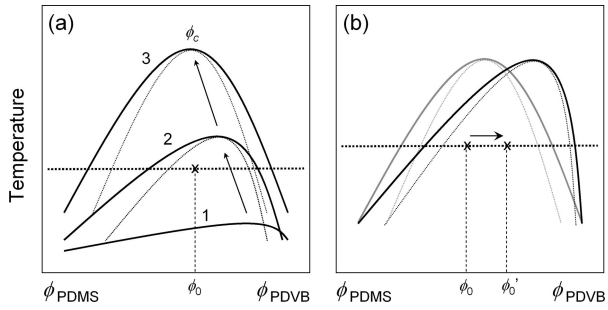


**Figure 4.** Schematic phase diagrams exhibiting the polymerization-induced phase separation. The solid and dotted lines represent the coexisting curve and the spinodal curve, respectively. (a) With the progress of polymerization, the coexisting curve moves upward (1 → 2 → 3), and the critical composition $\phi_c$ also moves in accordance with Equation (3) (see in the text). One example of starting composition $\phi_0$ is denoted as the symbol "×". (b) With a higher degree of polymerization of PDMS, the starting composition where bicontinuous morphology can be obtained shifts toward higher DVB region ($\phi_0 \rightarrow \phi_0'$).

Figure 4a. The critical composition $\phi_{i,c}$ is calculated with the condition

$$\frac{\partial^2 G}{\partial \phi^2} = \frac{\partial^3 G}{\partial \phi^3} = 0 \tag{2}$$

and hence,

$$\phi_{1,c} = \left(\frac{P_2}{P_1 + P_2}\right)^{1/2} \tag{3}$$

The parameters $P_1$ can be roughly estimated to increase from 1 up to 100 (∼[DVB]/[BTEE]) and $P_2$ are 120−135 for PDMS-10k and 810−880 for PDMS-65k, respectively. The critical composition $\phi_{i,c}$ therefore is initially ∼1 and become smaller with increasing $P_1$, but always keeps larger than 0.5. A starting composition $\phi_0$ (labeled as "×" in Figure 4) is located in the single phase region in the initial state 1. With the progress of polymerization, the coexisting curve rises to higher temperature, meaning extended instability due to the loss of free energy of mixing (state 2). Increasing PDMS in the starting composition further makes the coexisting curve upward (such as state 3). To obtain bicontinuous morphology, $\phi_0$ must be located at where the fraction of one phase is not far from 0.5 (near the symmetric composition). Oppositely, increasing TMB enhances the mutual compatibility and suppresses the rise of the coexisting curve. In the case of PDMS with higher molecular weight (i.e., larger $P_2$), the critical point moves toward more PDVB-rich region as confirmed from eq 3. The [PDMS]/[DVB] ratio in the starting solution also should be smaller in order to obtain bicontinuous morphology ($\phi_0'$ in Figure 4b), which is consistent with the experimental result shown in Figure 3.

The macropore size and volume data obtained by mercury porosimetry are shown in Figure 5. It is confirmed from part a that only the pore size changes while the total pore volume holds almost constant when the amounts of PDMS-10k is varied while keeping the solvent amount fixed. This situation can be qualitatively explained as follows: Since the contact enthalpy between PDMS and PDVB will increase with increasing concentration of PDMS, the free energy of mixing in eq 1 will increase. Thus, the coexisting curve in Figure 4 moves upward (to upper left, precisely). Since the starting composition is to be moved to the left with increasing concentration of PDMS, the volume relation between PDMS- and PDVB-rich phases hardly changes. Thus the concentration of PDMS only changes the pore size. Note that the small decrease in pore volume for the sample L775-8 may be attributed to the change in the phase fraction due to the further increase of the coexisting curve. On

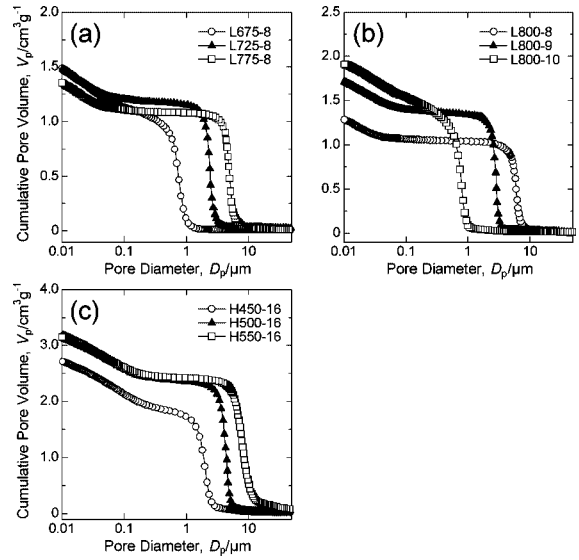


**Figure 5.** Cumulative pore volume and pore size distribution data obtained by mercury porosimetry: (a, c) varying only PDMS concentration, and (b) varying only TMB concentration. Parts a and b are results from the PDMS-10k system, and part c is the result from the PDMS-65k system.

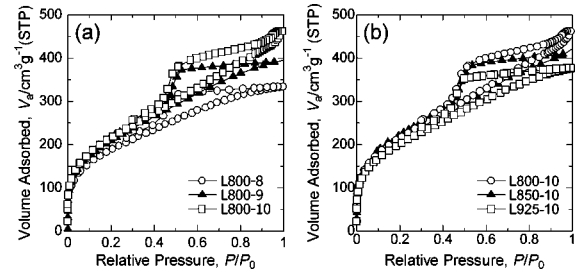


**Figure 6.** Nitrogen adsorption−desorption isotherms of the samples: (a) varying only TMB concentration and (b) varying only PDMS concentration. Increasing amount of TMB makes the pore volume larger, while increasing amount of PDMS-10k makes the pore volume smaller. See also Table 2.

the other hand, pore size becomes smaller and pore volume becomes larger with increasing amount of TMB as shown in part b. Since TMB is considered to be the good solvent in the present system, it would be distributed in the both phases in the phase-separating and gelling solution (even though the distribution may not be even). But it eventually will be excluded from the PDVB-rich phase by syneresis due to the cross-linking and will be thrust into the PDMS-rich fluidic phase to determine the total pore volume. In this way, the total pore volume is mainly determined by the amount of TMB, and it should be noted that varying TMB also affects the pore size. It therefore is possible to obtain dried gels which have the similar pore size and different pore volumes by changing both amounts of TMB and PDMS adequately (simultaneously increase or decrease both PDMS and TMB). Moreover, it can be confirmed that the pore volume of the gels can be made larger by using PDMS-65k as exhibited in Figure 5c. This is because the starting compositions leading to the bicontinuous macroporous morphology are shifted toward the region of higher concentration of TMB as explained above, and thus total pore volume can be made larger. In this case, similar to part a, pore volume should become almost constant for all the samples; however, pore volume for the sample H450-16 is exceptionally small. This is due to the larger shrinkage for the sample with smaller pore size. The longer PDMS chains disturb the polymerization of DVB to some extent by entangling around and more unreacted vinyl groups would

**Table 2. Properties of the Skeletal Pores Obtained from the Nitrogen Sorption Measurements**

| code | BET surface area/$m^2$ $g^{-1}$ | total pore volume/$cm^3$ $g^{-1}$ |
|---|---|---|
| L800-8 | 668 | 0.372 |
| L800-9 | 721 | 0.461 |
| L800-10 | 749 | 0.562 |
| L850-10 | 730 | 0.495 |
| L925-10 | 705 | 0.434 |
| H400-16 | 690 | 0.720 |
| H525-16 | 863 | 0.989 |
| L600-6 | 680 | 0.368 |
| L700-8 | 763 | 0.463 |
| L700-10 | 390 | 0.429 |

be left, which results in lower cross-linking density. The resultant softer networks consequently shrink more due to the interfacial tension induced by the drying solvent. Also, since the concentration of DVB in a starting solution in PDMS-65k system is lower than that in PDMS-10k system, bulk density of the resultant gel is smaller, which results in more shrinkage as well.

**3.2. Formation Mechanism of Smaller Pores (Skeletal Pores) Inside the PDVB Skeletons.** Inside the gel skeletons consisting macropores, smaller pores (hereafter referred as "skeletal pores") with various sizes are found by nitrogen sorption measurements. In this section, the formation mechanism of skeletal pores is deduced and factors affecting the skeletal pore characteristics are discussed.

In Figure 6, it is given that the nitrogen adsorption−desorption isotherms of PDVB gels prepared with different concentrations of TMB in part a and PDMS-10k in part b. Also, Table 2 lists values of the BET surface area and total pore volume determined by the BJH method. In each isotherm, the continuous increase of adsorption from the low to high relative pressure range and the appearance of hysteresis loop between adsorption and desorption branches suggest the existence of pores with various sizes (meso- and macropores) inside the PDVB skeletons. This is supported by the FE-SEM image of the skeleton of the sample L700-8 as shown in Figure 7. The steep increase in adsorbed volume at the very low relative pressure region ($P/P_0 < 0.01$) can be attributed to the existence of micropores. Here, we denote the pores in accordance with the IUPAC recommendation; macropores are larger than 50 nm in diameter, mesopores are between 2 and 50 nm, and micropores are less than 2 nm.[35] In Figure 6a, increasing the amount of TMB makes the skeletal pore volume larger as can be confirmed in Table 2. Conversely, increasing the amount of PDMS makes the pore volume smaller as depicted in part b and listed in Table 2. Note that the increase in adsorption at higher relative pressures in the sample L800-10 is due to the small macropores formed by the early stage of phase separation. In part a, macroporous morphologies of the samples L800-9 and L800-8 are "bicontinuous" and "aggregate of particles", respectively. Also in part b, L850-10 and L925-10 are respectively "bicontinuous" and "aggregate of particles". In the chemical cooling, being different from the physical cooling, the quench depth continues to become deeper by the continuous progress of polymerization.[36−38] Besides, in decreasing TMB or increasing PDMS, immiscibility becomes stronger and it would lead to the deeper quench. During this period, further phase separation (secondary phase separation or double phase separation)[39−41] will take place inside the gelling phase (and also in the PDMS-rich fluidic phase) with the progress of further polymerization because of the high immiscibility between PDVB and PDMS as described above.[34] For the gels with aggregate of particles such as L800-8 and L925-10, phase separation starts earlier enough prior to gelation. Additionally, since phase separation starts at when DP of DVB is relatively small and

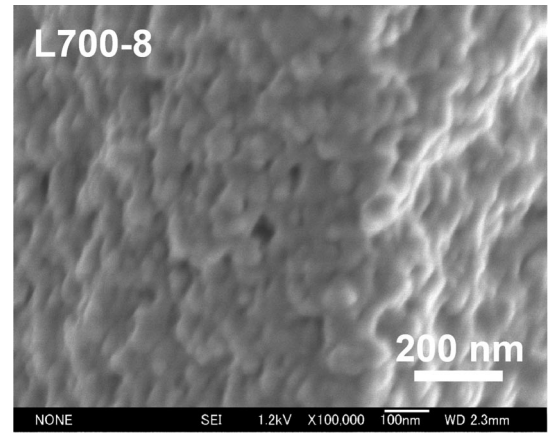


**Figure 7.** FE-SEM image of the sample L700-8 showing various sizes of skeletal pores.

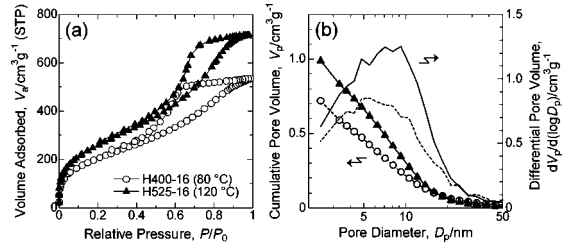


**Figure 8.** (a) Nitrogen adsorption−desorption isotherms of the samples H400-16 prepared at 80 °C and H525-16 prepared at 120 °C. (b) Cumulative pore volume and pore size distribution derived from the BJH method using the adsorption branch of each isotherm in part a. The solid and broken distribution curves are for the sample H525-16 (120 °C) and H400-16 (80 °C), respectively.

viscosity of the system therefore would remain low during phase separation. In such a system, secondary phase separation would proceed well and the compositions in both phases become more close to the equilibrium ones owing to the long phase separation time and low viscosity. On the other hand, for the bicontinuous gels such as L800-9 and L850-10, the phase separation time is shorter, and moreover, viscosity during phase separation is higher. Secondary phase separation in both phases thus proceeds less intensely and both phases cannot follow the equilibrium compositions. That is, the structures formed by secondary phase separation are not fully relaxed and the larger amount of the skeletal pores remains as a result. Size of the skeletal pores may also be determined by secondary phase separation. They are however difficult to control because of the complex aspects of secondary phase separation: Quench depth and reaction rate as well as the phase separation time and viscosity largely affect the behavior of secondary phase separation.[36,37] It is worth noting that an additional reason for increasing skeletal pore volume with increasing TMB that can be confirmed from Figure 6a is syneresis inside the skeletons considering from analogy with the first phase separation that forms macropores.

Next, we consider the situation where PDMS-65k is used instead of PDMS-10k. When PDMS with higher molecular weight is included, the skeletal pores are increased as shown in Figure 8 and Table 2. The two samples were prepared at the different temperatures and are selected because these two are the similar morphology of bicontinuous structure. For the sample prepared at 80 °C (H400-16), the adsorbed volume is slightly increased compared to samples prepared with PDMS-10k, indicating more skeletal pore volume as shown in part a. For the sample prepared at 120 °C (H525-16), the adsorbed volume is drastically increased, and moreover, an inflection point, which is resulted from the capillary condensation in the pores with a

narrow pore size distribution, can be recognized around at the relative pressure 0.75. The driving force of secondary phase separation is larger for PDMS-65k system due to the higher incompatibility between PDVB and PDMS. Since the degree of polymerization of PDVB at the onset of phase separation is smaller for PDMS-65k system, the phase separation time is also longer, during which secondary phase separation should proceed and reach closer to the coexisting composition. This would make pore volume smaller; however, the increasing amount of solvent increases the skeletal pore volume by syneresis. For this reason, the skeletal pore volume for the sample H400-16 is larger than those prepared with PDMS-10k (see Table 2). In the case of H525-16 prepared at 120 °C, the faster polymerization rate, i.e., shorter phase separation time, makes the skeletal pore volume larger with the same reason discussed in Figure 6. Namely, due to the fast polymerization rate, the compositions in the separated phases cannot keep up with the equilibrium compositions that continue to become much richer in PDMS or PDVB. Thus, the transient structure of secondary phase separation will be frozen by gelation with leaving larger pore volume. The higher tendency for secondary phase separation in PDMS-65k system allows the more distinct pores and narrower pore size distribution as exhibited in Figure 8b. Another possibility for the larger pore volume is that the high temperature such as 120 °C causes the termination reactions due to the steep increase of radical concentration at the beginning of the reaction.[42−44] This consequently increase the PDI of PDVB and dead cross-linked polymer particles with a certain size may be generated. In-between such particles or the regions with higher cross-linking density compared to surroundings in the networks, pores would be generated, resulting in increasing skeletal pores.

From above discussions, it can be summarized that dried gels with more coarsened phase-separated structures have less skeletal pores because of the longer phase separation time during which the system remains fluidic. The higher molecular weight of PDMS would enhance secondary phase separation, leading to the more distinct skeletal pores. Also, the larger amount of TMB increases the skeletal pore volume. Since the higher temperature shortens the phase separation time, the remaining skeletal pores are increased. In the next section, we will further discuss the pore formation inside the skeletons with varied concentrations of BTEE and AIBN.

**3.3. Effects of Varying BTEE and AIBN Concentrations.** In this section, we further discuss the factors that affect macropores and skeletal pores. Concentrations of BTEE and AIBN alter the molecular weight of growing polymer and polymerization kinetics, respectively. These factors naturally affect the phase separation behaviors, or in other words, characters of macropore and skeletal pore are changed.

As for macroporous morphology, it was also found that increasing concentrations of BTEE and AIBN made the compositional area with bicontinuous structure shift toward the lower concentration of DVB as depicted in Figure 9a (see also Figure 3 for comparison). This behavior resembles the case of increasing molecular weight of PDMS. On increasing BTEE concentration, since the population of growing polymers increases, the number-average molecular weight $M_n$ of PDVB will be decreased when considering the analogy with the case of linear polymers. This situation itself makes the phase separation tendency weaker due to the increase of the entropy of mixing (increasing the first term in eq 1) arising from the lower $M_n$. In this case, however, longer time is required for gelation (ca. 1.2 times when BTEE and AIBN are doubled in a nonphase-separating system). Since longer time until gelation allows further coarsening, the stronger phase separation tendency is observed. Reversely, decreasing amounts of BTEE and AIBN made the phase separation tendency smaller, viz. the phase

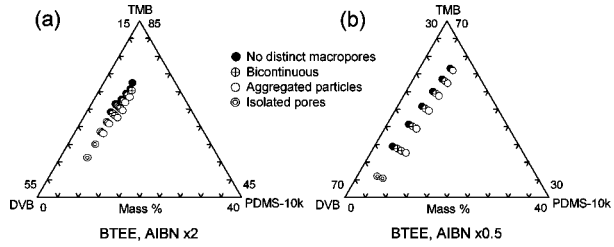


**Figure 9.** Triangular plots showing composition-morphology relationships with varying concentrations of BTEE and AIBN. (a) Both BTEE and AIBN are doubled (i.e., 2 mol % and 1 mol % of DVB, respectively), and (b) both BTEE and AIBN are halved (i.e., 0.5 mol % and 0.25 mol % compared to DVB, respectively).

separation region is shifted to higher concentration of DVB. Varying concentration of AIBN alone while that of BTEE is fixed made only a little effect on the macroporous structure of PDVB. This result indicates that what gives a major effect on the polymerization of DVB is the concentration of BTEE. Addition of AIBN or other radical sources allows the faster living polymerization or polymerization in milder conditions.[25,42−44] The concentration of AIBN contributes only to the initiation step and does not to the chain-propagating step. Once radical species are generated from AIBN, DVB molecules predominantly undergo degenerative-transfer-mediated polymerization promoted by organotellurium dormant species. On increasing AIBN, the polymerization rate becomes faster and the morphological formation by phase separation takes place somewhat later compared to gelation. On decreasing AIBN alone, conversely, the slower polymerization formed the a little more coarsened morphologies. It is known that increasing initiator concentration in other living radical polymerization techniques makes the polymerization rate constant and the polydispersity index (PDI) slightly larger,[42−44] while PDI is hardly influenced by the addition of a radical initiator in TERP due to the fast degenerative transfer.[25] Besides, since the resultant molecular weight is not changed with the addition of azo initiator, the phase separation tendency is not largely affected in the present case. Faster (slower) polymerization kinetics therefore would make phase separation to be a little less (more) proceeded in the same [DVB]/[TMB]/[PDMS] ratio when more (less) AIBN is employed. In the case of varying only the BTEE concentration, on the other hand, the phase separation tendency is very similar to the case of varying both BTEE and AIBN. In fact, on varying both BTEE and AIBN, a combined effect from independently varying BTEE and AIBN are apparent. That is, the changes in molecular weight and kinetics simultaneously affect the final morphology.

It is also worth mentioning that the change in skeletal pores with varying BTEE and AIBN concentrations. As described above, varying only the AIBN concentration hardly affects the molecular weight of PDVB, and thus the phase separation behavior is also hardly changed. Consequently, the properties of the skeletal pores are not significantly changed. When the concentration of BTEE is varied, on the other hand, a visible change has been observed. Figure 10 shows the nitrogen sorption isotherms for the samples with different BTEE concentrations. As the adsorption volume changes with the progress of phase separation, the samples shown in Figure 10 were selected because they were prepared from different compositions but have comparable macroporous morphologies. However, as noted above, the larger amount of TMB would give rise to the pore volume. The adsorption curves therefore should be increased in the order of L600-6 (0.5 mol % BTEE), L700-8 (1 mol % BTEE) and L700-10 (2 mol % BTEE). In practice, however, the adsorption of L700-10 (2 mol % BTEE) is exceptionally low. With higher concentration of BTEE, the larger number of

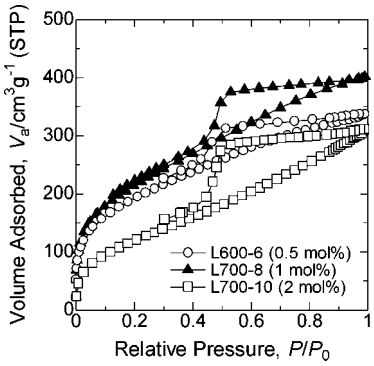


**Figure 10.** Nitrogen adsorption−desorption isotherms of the samples with different concentrations of BTEE (0.5, 1, and 2 mol % relative to DVB) while other components are fixed. The exceptional low adsorption for the sample L700-10 (2 mol %) implies the suppression of secondary phase separation due to the lower $M_n$ of PDVB.

polymerized species with lower $M_n$ is formed before gelation as discussed above. These small species would suppress secondary phase separation, resulting in the smaller volume of micro- and mesopores (see also Table 2). The smaller volume of micropores largely contributes the smaller value of specific BET surface area. When both BTEE and AIBN are simultaneously varied, a combined effect appears.

## 4. Conclusion

In the present paper, we have shown that phase separation (spinodal decomposition) can be induced in the homogeneous networks derived from organotellurium-mediated living radical polymerization (TERP) of DVB in the solvent TMB, and well-defined macroporous bicontinuous morphology can be consequently obtained after removing the solvent. With the addition of a polymeric agent PDMS that remains unreacted throughout the reaction, polymerization-induced phase separation takes place between PDMS-rich and PDVB-rich phases. The resultant porous dried gels possess two levels of pores; macropores formed by phase separation and skeletal pores by secondary phase separation inside the PDVB skeletons, which consists macropores.

By changing various parameters such as concentration and molecular weight of PDMS, concentrations of TMB, BTEE and AIBN, and reaction temperature, properties of both macro- and skeletal pores are altered as a result of a varied polymerization behavior. The increased concentration of PDMS in the starting solution enhances the phase separation tendency as expected. More coarsened macropores with larger sizes are therefore obtained. The enhanced phase separation tendency, on the other hand, suppresses secondary phase separation in the skeletons, which leads to the less skeletal pores. With increasing amount of the solvent TMB, phase separation is inhibited, which suggests that TMB acts as the good solvent and enhances the mutual solubility of PDVB and PDMS. The good solvent must be distributed in the both phases, however, it will be excluded from the PDVB-rich gelling phase by syneresis. Since the same is true in secondary phase separation in the skeletons, the total pore volume is mainly determined by the amount of the solvent. On changing the concentration of BTEE, the phase separation behavior is influenced because $M_n$ of PDVB species is varied. Since higher concentration of BTEE gives rise to the number of PDVB species with lower $M_n$, gelation becomes slower. Since phase separation much proceeds during the slow gelation, more coarsened macroporous structure is obtained. The skeletal pores are reduced because of the weaker tendency of secondary phase separation. Polymerization kinetics is affected by the concentration of AIBN. Because increasing AIBN raises the reaction rate and gelation takes place much earlier with respect to the onset of phase separation, macropore size becomes somewhat smaller.

As reported previously, other living polymerization techniques such as NMP and ATRP also afford the morphogenesis by spinodal decomposition in the course of homogeneous network formation. The present results strongly support the idea that the heterogeneous networks derived from conventional free radical polymerization avoid the occurrence of isotropic spinodal decomposition, which, on the other hand, can be induced in the more homogeneous networks derived from living polymerization. The relationship between homogeneity of the networks and the occurrence of isotropic spinodal decomposition is left for the future study.

**Acknowledgment.** The present work was supported by the Grant-in-Aid for Young Scientists (B) (No. 20750177) from the MEXT, Japan, and was partly supported by a Grant for Practical Application of University R&D Results under the Matching Fund Method from New Energy and Industrial Technology Development Organization (NEDO), Japan. Also acknowledged is the Global COE Program "International Center for Integrated Research and Advanced Education in Materials Science" (No. B-09) of the Ministry of Education, Culture, Sports, Science and Technology (MEXT) of Japan, administrated by the Japan Society for the Promotion of Science (JSPS).

## References and Notes

(1) Webster, O. W. *Science* **1991**, *251*, 887–893.
(2) Ide, N.; Fukuda, T. *Macromolecules* **1997**, *30*, 4268–4271.
(3) Ide, N.; Fukuda, T. *Macromolecules* **1999**, *32*, 95–99.
(4) Jiang, C.; Shen, Y.; Zhu, S.; Hunkeler, D. *J. Polym. Sci., Part A* **2001**, *39*, 3780–3788.
(5) Norisuye, T.; Morinaga, T.; Tran-Cong-Miyata, Q.; Goto, A.; Fukuda, T.; Shibayama, M. *Polymer* **2005**, *46*, 1982–1994.
(6) Yu, Q.; Zhou, M.; Ding, Y.; Jiang, B.; Zhu, S. *Polymer* **2007**, *48*, 7058–7064.
(7) Gao, H.; Min, K.; Matyjaszewski, K. *Macromolecules* **2007**, *40*, 7763–7770.
(8) Gao, H.; Li, W.; Matyjaszewski, K. *Macromolecules* **2008**, *41*, 2335–2340.
(9) Yu, Q.; Qin, Z.; Li, J.; Zhu, S. *Polym. Eng. Sci.* **2008**, *48*, 1254–1260.
(10) Bastide, J.; Leibler, L. *Macromolecules* **1988**, *21*, 2649–2651.
(11) Chiu, Y. Y.; Lee, J. *J. Polym. Sci., Part A* **1995**, *33*, 257–267.
(12) Chiu, Y. Y.; Lee, J. *J. Polym. Sci., Part A* **1995**, *33*, 269–283.
(13) Norisuye, T.; Kida, Y.; Masui, N.; Tran-Cong-Miyata, Q.; Maekawa, Y.; Yoshida, M.; Shibayama, M. *Macromolecules* **2003**, *36*, 6202–6212.
(14) Shibayama, M. *Bull. Chem. Soc. Jpn.* **2006**, *79*, 1799–1819.
(15) Okay, O. *Prog. Polym. Sci.* **2000**, *25*, 711–779.
(16) Peters, E. C.; Petro, M.; Svec, F.; Fréchet, J. M. J. *Anal. Chem.* **1997**, *69*, 3646–3649.
(17) Gusev, I.; Huang, X.; Horváth, C. *J. Chromatogr. A* **1999**, *855*, 273–290.
(18) Krajnc, P.; Leber, N.; Stefanec, D.; Kontrec, S.; Podgornik, A. *J. Chromatogr. A* **2005**, *1065*, 69–73.
(19) Svec, F. *J. Sep. Sci.* **2005**, *28*, 729–745.
(20) Buchmeiser, M. R. *Polymer* **2007**, *48*, 2187–2198.
(21) Kanamori, K.; Nakanishi, K.; Hanada, T. *Adv. Mater.* **2006**, *18*, 2407–2411.
(22) Kanamori, K.; Hasegawa, J.; Nakanishi, K.; Hanada, T. *Macromolecules* **2008**, *41*, 7186–7193.
(23) Yamago, S.; Iida, K.; Yoshida, J. *J. Am. Chem. Soc.* **2002**, *124*, 2874–2875.
(24) Yamago, S.; Iida, K.; Yoshida, J. *J. Am. Chem. Soc.* **2002**, *124*, 13666–13667.
(25) Goto, A; Kwak, Y.; Fukuda, T.; Yamago, S.; Iida, K.; Nakajima, M.; Yoshida, J. *J. Am. Chem. Soc.* **2003**, *125*, 8720–8721.
(26) Yamago, S. *J. Polym. Sci., Part A* **2006**, *44*, 1–12.
(27) Braunecker, W. A.; Matyjaszewski, K. *Prog. Plym. Sci.* **2007**, *32*, 93–146.
(28) Hashimoto, T.; Itakura, M.; Hasegawa, H. *J. Chem. Phys.* **1986**, *85*, 6118–6128.
(29) Hashimoto, T.; Itakura, M.; Shimidzu, N. *J. Chem. Phys.* **1986**, *85*, 6773–6786.

(30) Flory, P. *J. Principles of Polymer Chemistry*; Cornell University Press: Ithaca, NY, 1971.
(31) Small, P. A. *J. Appl. Chem.* **1953**, *3*, 71–80.
(32) Ashworth, A. J.; Price, G. J. *Macromolecules* **1986**, *19*, 362–363.
(33) Nose, T. *Polymer* **1995**, *36*, 2243–2248.
(34) de Gennes, P.-G. *Scaling Concepts in Polymer Physics*; Cornell University Press: Ithaca, NY, 1979.
(35) Sing, K. S. W.; Everett, D. H.; Haul, R. A. W.; Moscou, L.; Pierotti, R. A.; Rouquérol, J.; Siemieniewska, T. *Pure Appl. Chem.* **1985**, *57*, 603–619.
(36) Ohnaga, T.; Chen, W.; Inoue, T. *Polymer* **1994**, *35*, 3774–3781.
(37) Inoue, T. *Prog. Polym. Sci.* **1995**, *20*, 119–153.
(38) Girard-Reydet, E.; Stautereau, H.; Pascault, J. P.; Keates, P.; Navard, P.; Thollet, G.; Vigier, G. *Polymer* **1998**, *39*, 2269–2280.
(39) Tanaka, H. *Phys. Rev. E* **1993**, *47*, 2946–2949.
(40) Tao, J.; Okada, M.; Nose, T. *Polymer* **1995**, *36*, 3909–3917.
(41) Sigehuzi, T.; Tanaka, H. *Phys. Rev. E* **2004**, *70*, 051504.
(42) Greszta, D.; Matyjaszewski, K. *J. Polym. Sci., Part A* **1997**, *35*, 1857–1861.
(43) Goto, A.; Fukuda, T. *Macromolecules* **1997**, *30*, 4272–4277.
(44) Yoshikawa, C.; Goto, A.; Fukuda, T. *Macromolecules* **2003**, *36*, 908–912.

MA802343A